Journal of Applied Physics

Sb-related defects in Sb-doped ZnO thin film grown by pulsed laser deposition

Cite as: J. Appl. Phys. **123**, 161525 (2018); https://doi.org/10.1063/1.4997510
Submitted: 25 July 2017 . Accepted: 18 October 2017 . Published Online: 03 November 2017

Caiqin Luo, Lok-Ping Ho, Fahad Azad, Wolfgang Anwand, Maik Butterling, Andreas Wagner, Andrej Kuznetsov, Hai Zhu, Shichen Su, and Francis Chi-Chung Ling

View Online Export Citation CrossMark

ARTICLES YOU MAY BE INTERESTED IN

A comprehensive review of ZnO materials and devices
Journal of Applied Physics **98**, 041301 (2005); https://doi.org/10.1063/1.1992666

Defect induced room temperature ferromagnetism in single crystal, poly-crystal, and nanorod ZnO: A comparative study
Journal of Applied Physics **123**, 161507 (2018); https://doi.org/10.1063/1.4986606

Identification of F impurities in F-doped ZnO by synchrotron X-ray absorption near edge structures
Journal of Applied Physics **123**, 161528 (2018); https://doi.org/10.1063/1.4997356

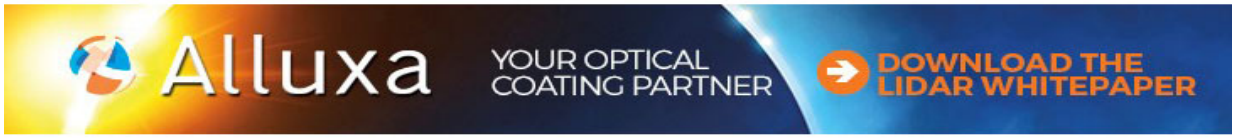

AIP Publishing

© 2017 Author(s).

Sb-related defects in Sb-doped ZnO thin film grown by pulsed laser deposition

Caiqin Luo,[1] Lok-Ping Ho,[1] Fahad Azad,[1] Wolfgang Anwand,[2] Maik Butterling,[2] Andreas Wagner,[2] Andrej Kuznetsov,[3] Hai Zhu,[4] Shichen Su,[1,5] and Francis Chi-Chung Ling[1,a)]

[1]*Department of Physics, The University of Hong Kong, Hong Kong, China*
[2]*Institute of Radiation Physics, Helmholtz-Zentrum Dresden-Rossendorf, Dresden, Germany*
[3]*Department of Physics, Oslo University, Oslo, Norway*
[4]*State Key Laboratory of Optoelectronic Materials and Technologies, School of Physics, Sun Yat-Sen University, Guangzhou, China*
[5]*Institute of Optoelectronic Material and Technology, South China Normal University, Guangzhou, China*

(Received 25 July 2017; accepted 18 October 2017; published online 3 November 2017)

Sb-doped ZnO films were fabricated on c-plane sapphire using the pulsed laser deposition method and characterized by Hall effect measurement, X-ray photoelectron spectroscopy, X-ray diffraction, photoluminescence, and positron annihilation spectroscopy. Systematic studies on the growth conditions with different Sb composition, oxygen pressure, and post-growth annealing were conducted. If the Sb doping concentration is lower than the threshold $\sim 8 \times 10^{20}\,\mathrm{cm}^{-3}$, the as-grown films grown with an appropriate oxygen pressure could be $n \sim 4 \times 10^{20}\,\mathrm{cm}^{-3}$. The shallow donor was attributed to the Sb_{Zn} related defect. Annealing these samples led to the formation of the Sb_{Zn}-$2V_{Zn}$ shallow acceptor which subsequently compensated for the free carrier. For samples with Sb concentration exceeding the threshold, the yielded as-grown samples were highly resistive. X-ray diffraction results showed that the Sb dopant occupied the O site rather than the Zn site as the Sb doping exceeded the threshold, whereas the Sb_O related deep acceptor was responsible for the high resistivity of the samples. *Published by AIP Publishing*. https://doi.org/10.1063/1.4997510

I. INTRODUCTION

ZnO, having a direct wide band gap of 3.4 eV and a large exciton energy of 60 meV, has received extensive attention because of its potential in a variety of applications including ultra-violet (UV) optoelectronics, transparent electronics, sensors, spintronics, etc.[1] Despite extensive efforts, the development of practical ZnO-based devices was deterred by the difficulty in achieving p-type doping.[2–4] Undoped ZnO materials are usually n-type in conductivity and degenerately n-type doping is easily obtained using dopants like Ga or Al. Hydrogen, intrinsic defects, and OH and their defect complexes[5–9] have also been suggested to be the shallow donors in ZnO materials. Group V elements being p-type dopants of ZnO have already been studied intensively.[1,10–13] With first principles calculation, Limijumnong *et al.*[14] showed that the Zn-substitutional defects X_{Zn} (X = P, As and Sb) were donors, and the O-substitutional defects X_O were deep acceptors. Because of the large size mismatch, theoretical calculation showed that X_{Zn} had lower formation energy than X_O. Moreover, the X_{Zn}-$2V_{Zn}$ defect complexes (X = P, As, and Sb) are a shallow acceptor with low formation energies.[14] An experimental study of conversion-electron emission channeling from the implanting radioactive ^{73}As confirmed that the majority of the implanted As is located at the Zn-site[15] and a similar result was also observed for Sb.[16] There were also experimental studies reporting the fabrication of p-type ZnO using these dopants (for example, Refs. 17–21). However, the p-type conductivity was not reliable. There were also disagreements on the formation of X_{Zn}-$2V_{Zn}$ in ZnO. Janotti and Van de Walle[22] argued that the formation of these defect complexes was unlikely from the energetic consideration and the entropic considerations for the formation of complexes comprising of three constituents. With *ab initio* calculation, Puchaia and Morgan[23] reported that X_i–$3V_{Zn}$ (i.e., the X interstitial surrounded by three V_{Zn}) was the most stable Group V dopant-vacancy complex in ZnO. It was a deep acceptor and could not contribute to the p-type conductivity.

In the present study, Sb-doped ZnO films were grown on c-plane sapphire by pulsed laser deposition (PLD). The as-grown Sb-doped ZnO samples were degenerately n^+-type having $n > 10^{20}\mathrm{cm}^{-3}$, and annealing at 750 °C lead to a dramatic decrease of the carrier concentration to $<10^{15}\mathrm{cm}^{-3}$. A comprehensive spectroscopic study including Hall effect measurements, X-ray photoelectron spectroscopy (XPS), X-ray diffraction (XRD), and positron annihilation spectroscopy (PAS) was performed with an attempt to understand the correlations between the defects and the carrier concentrations.

II. EXPERIMENTAL

The undoped ZnO and Sb-doped ZnO thin films were grown on the c-plane sapphire substrate using the pulsed laser deposition (PLD) method. The target was ZnO:Sb_2O_3 with different Sb weight ratios of 0.5%, 1%, 2%, and 3%. The background pressure was $\sim 10^{-4}$ Pa. An excited KrF excimer laser (wavelength = 248 nm, a pulse energy of 300 mJ, and frequency = 2 Hz) was employed to ablate the target. During

a)Email: ccling@hku.hk

the growth, the substrate temperature was kept at 350 °C, and two oxygen pressures were adopted (P (O_2) = 1.3 and 5 Pa) during the growth. The thickness of the film was about 300 nm. Isochronal annealing was performed in a tube furnace for 40 min in argon at 600, 750, and 900 °C, respectively. The sample was put into the furnace after the temperature was stable at the desired value. The ramp down rate was around 8 °C/min. The XRD study was conducted by using a Phillips D5000 and Bruker D8 advance (high resolution) X-ray diffractometer with the Cu K α line. The Hall measurement was conducted at room temperature using the van der Pauw configuration by the Accenet HL-5500PC system. The XPS measurements were carried out by using the VG MICROTECH MT500 XPS system. For the SIMS measurement, the IONTOF TOF-SIMS V spectrometer was used. PAS measurement was carried out with a 35 keV mono-energetic positron beam. A high purity Ge detector and the corresponding nuclear electronics which had an energy resolution of 1.1 keV for the 514 keV line were used to collect the gamma ray energy spectra of the annihilation gamma photons. The window for obtaining the S parameter was (511 ± 0.92) keV.

III. RESULTS

A. Structural characterization

Figure 1 shows the diffraction patterns of the as-grown undoped ZnO and the ZnO:Sb samples with Sb = 1%, 2%, and 3% obtained from the HRXRD measurements with the intensity plotted in the log scale. The major peaks found in all these spectra are the (002) and (004) peaks, and other three peaks (100), (101), (103), and (200) having negligibly small intensities (~100 times less than that of the (002) peak) were also identified. It is also noticed that no extra peaks in the Sb-doped ZnO spectra other than those identified in the undoped ZnO spectrum were found. All these results show that the films have a wurtzite structure orientated along the c-axis without any significant formation of Sb phases within the spectrometer resolution. Moreover, (002) and (004) peaks shifting to a low angle is observed for the Sb-doped ZnO sample with Sb = 3%. This observation will be discussed in the upcoming paragraphs. Figure 2 shows the XRD spectra of the Sb-doped ZnO samples grown with the oxygen pressure P (O_2) = 1.3 Pa with different post-growth annealing treatments (namely, as-grown, 600, 750 and 900 °C). The magnified (002) peaks are also shown in the inset of the figure. New phase was not found in the XRD spectra during the annealing process. The (002) peaks shift to a low angle for the samples annealed at 750 and 900 °C and this will be discussed later.

The full width half maximum (FWHM) of the (002) peaks for the different ZnO:Sb samples grown with P(O_2) = 1.3 Pa is shown in Fig. 3(a). The FWHM of the as-grown ZnO:Sb samples increases slightly from 0.241° to 0.244° as the Sb composition increases from 1% to 2%, and then an abrupt increase is observed as the Sb composition further increases to 3%, implying the deterioration of the crystalline quality by high level Sb doping. An annealing study on the samples with a Sb composition of 2% shows that an abrupt decrease of FWHM is induced by annealing at 750 °C, which is possibly associated with the improvement in the crystalline quality. The lattice constants of the samples were also calculated and the results are shown in Fig. 3(b). The lattice constants of the as-grown Sb-doped ZnO films doped with 1% and 2% Sb are the same as 5.21 Å. A dramatic increase

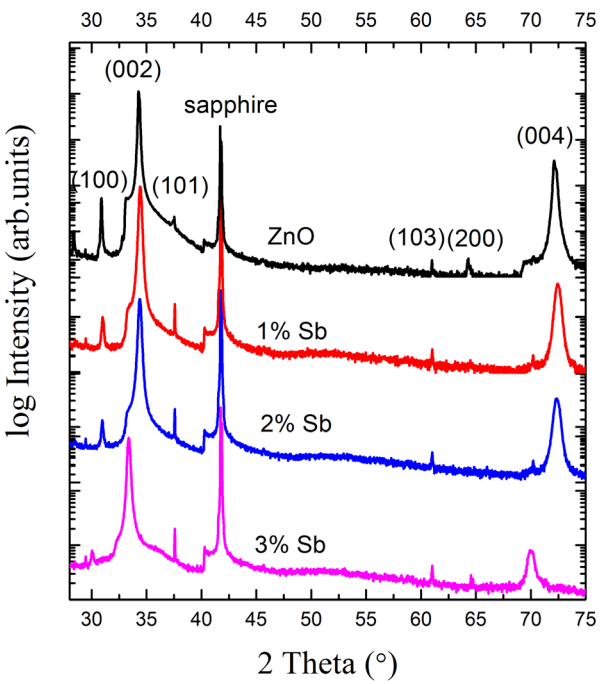

FIG. 1. The HRXRD spectra of the as-grown undoped and ZnO:Sb samples grown with P(O_2) = 1.3 Pa.

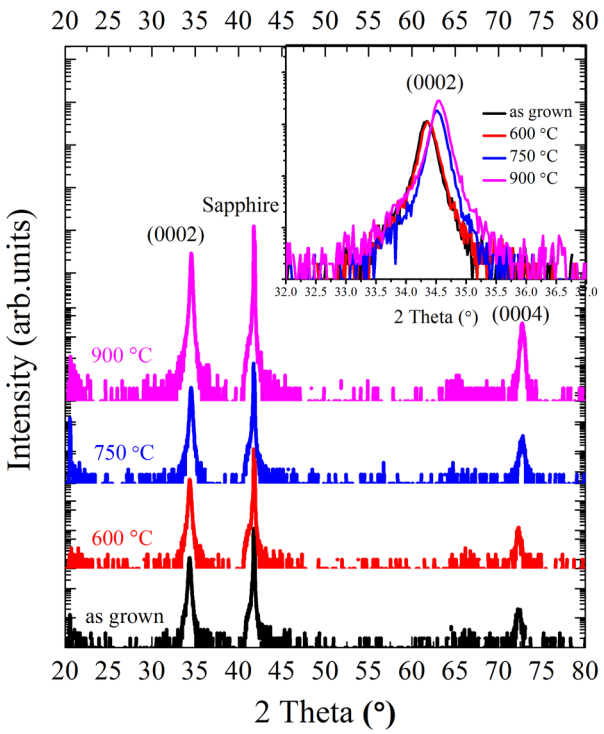

FIG. 2. The XRD spectra of the Sb doped ZnO thin films grown on sapphire annealed at different temperatures. The inset shows the magnified (002) peaks of the spectra. The PLD growths were performed with the oxygen pressure of 1.3 Pa.

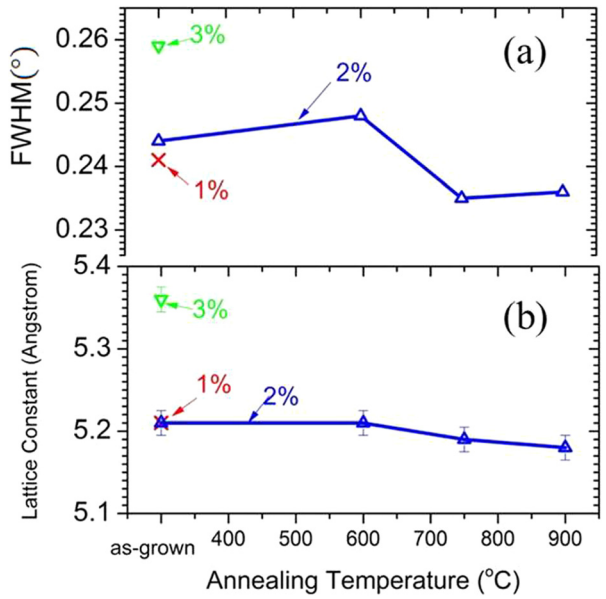

FIG. 3. (a) The FWHM of the ZnO (002) peaks in the XRD spectra and (b) the lattice constant for the ZnO:Sb (2%) samples as a function of the annealing temperature. The corresponding FWHM's and lattice constant for the as-grown ZnO:Sb samples with Sb compositions of 1% and 3% were also included. All the samples were grown with the oxygen pressure of 1.3 Pa.

of the lattice constant to 5.36 Å was observed as the Sb composition further increased to 3%. The effect of annealing on the lattice constant was shown for the case of Sb composition equal to 2%. A very slight decrease of the lattice constant (though within the measurement error) from 5.21 Å to 5.18 Å occurred after annealing at 750 °C.

SIMS measurement was carried out to obtain the depth profile of Sb for the ZnO:Sb (2%) sample grown with P (O_2) = 1.3 Pa in the as-grown state and that annealed at 900 °C. The SIMS depth profiles showed a rather uniform distribution of Sb throughout the whole film, and no segregation was observed. The atomic concentration of Sb in the ZnO:Sb samples grown with the different Sb compositions in the target (by weight) was measured by XPS, and the results are plotted in Fig. 4. The Sb concentration of the as-grown Sb-doped sample increased linearly with the Sb composition in the target, from $1 \times 10^{20}\,\mathrm{cm}^{-3}$ to $1 \times 10^{21}\,\mathrm{cm}^{-3}$, as the Sb composition increased from 0.5% to 3%.

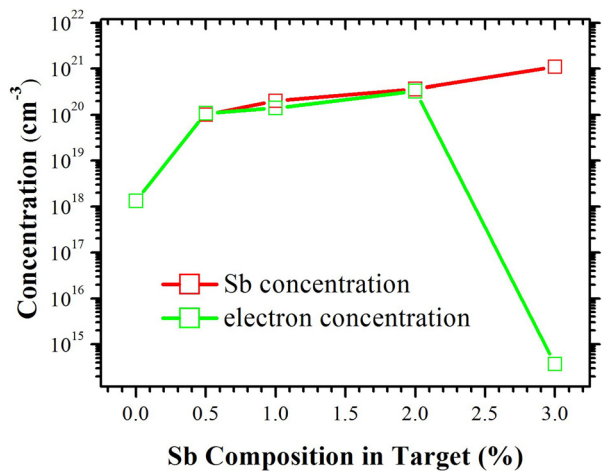

FIG. 4. The electron concentration and Sb concentration measured by Hall measurement and XPS, respectively, are plotted against the Sb composition (in weight) of the target used for the PLD growth.

B. Hall measurements

Hall measurements showed that all the Sb-doped ZnO samples exhibited n-type conductivity. Figure 4 shows the electron concentration as a function of the Sb composition (by weight in the target) for the as-grown Sb-doped ZnO samples grown with P (O_2) = 1.3 Pa. For the undoped ZnO sample, the electron concentration was $\sim 1 \times 10^{18}\,\mathrm{cm}^{-3}$. With the Sb composition $\leq$ 2%, doping more Sb had the effect of increasing the electron concentration and its value was effectively equal to the Sb concentration, i.e., increasing from $1 \times 10^{20}\,\mathrm{cm}^{-3}$ to $3 \times 10^{20}\,\mathrm{cm}^{-3}$, while the Sb composition increased from 0.5% to 2%. This strongly suggests that the shallow donor is related to the Sb dopant. However, further increasing the Sb composition to 3% dramatically decreased the electron concentration to $\sim 4 \times 10^{14}\,\mathrm{cm}^{-3}$ and the sample became highly resistive, though the concentrations of Sb increased to $1 \times 10^{21}\,\mathrm{cm}^{-3}$. The dramatic drop in electron concentration could be due to formation of a compensation defect and/or the change of the Sb-related shallow donor microstructure as the Sb composition is high.

Figure 5 shows the electron concentration as a function of the oxygen pressure during growth P (O_2) for the as-grown ZnO:Sb (1%) sample. For the sample grown with no oxygen, the carrier concentration was $\sim 5 \times 10^{20}\,\mathrm{cm}^{-3}$. Increasing P ($O_2$) had the effect of decreasing the electron concentration. As P (O_2) reached 1.3 Pa, the electron concentration decreased to the saturated value of $\sim 9 \times 10^{19}\,\mathrm{cm}^{-3}$.

Figures 6(a) and 6(b) show the electron concentration as a function of the annealing temperature, respectively, for the undoped ZnO, as well as the ZnO:Sb (2%) samples grown with the growth oxygen pressures P (O_2) = 1.3 and 5 Pa. For the Sb-doped samples, the as-grown samples were n-type conducting and had carrier concentrations of $4 \times 10^{20}\,\mathrm{cm}^{-3}$ and $1 \times 10^{19}\,\mathrm{cm}^{-3}$ for the samples grown with P (O_2) = 1.3 and 5 Pa, respectively, which were significantly higher than those of the undoped samples. The two Sb-doped ZnO samples grown with the different P (O_2) showed similar features. After annealing at 750 °C, the electron concentrations of the

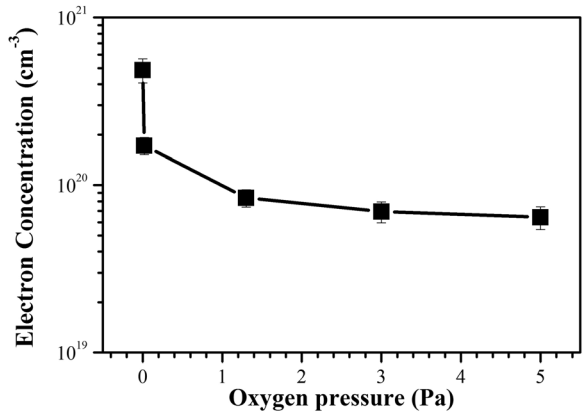

FIG. 5. The electron concentration of the as-grown ZnO:Sb (1%) sample as a function of the oxygen pressure during growth.

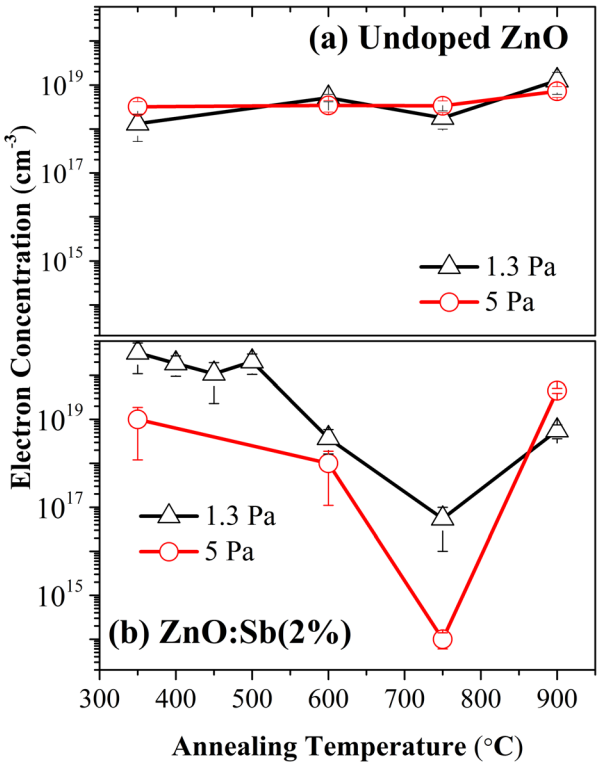

FIG. 6. The electron concentration as a function of the annealed temperature for (a) undoped ZnO samples and (b) Sb-doped ZnO (Sb = 2% by weight) samples grown on the sapphire using the PLD method. The films were grown with oxygen pressures of 1.3 and 5 Pa, respectively.

Sb-doped samples grown with P (O_2) = 1.3 and 5 Pa dropped significantly to values of $\sim 10^{17}\,cm^{-3}$ and $\sim 10^{14}\,cm^{-3}$, respectively, corresponding to the decreasing of factors of 4000 and 10^5. For the undoped samples, the electron concentration remained in a narrow range from 10^{18} to $10^{19}\,cm^{-3}$ irrespective of the P (O_2) and the annealing temperature up to 900 °C. This implies the abrupt thermally induced decrease in the carrier concentration as observed in the Sb-doped ZnO samples associated with the physics or chemistry of the Sb dopant.

Temperature dependent Hall measurements were performed on the as-grown Sb-doped ZnO (Sb = 2%) sample grown with P (O_2) = 1.3 Pa at temperature ranging from 10 K to 300 K, and the carrier concentration against the temperature data is shown in Fig. 7. At T = 10 K, the electron concentration was $\sim 2 \times 10^{19}\,cm^{-3}$. Increasing the temperature led to more shallow donors being ionized and thus resulted in the increase of the electron concentration. As the temperature increased to ~150 K, the electron concentration saturated at $\sim 2 \times 10^{20}\,cm^{-3}$ as a majority of the shallow donors became ionized. The ionization energy of the shallow donor was estimated by fitting the Arrhenius plot of the electron concentration in the temperature range of 10 K to 150 K (shown in the inset of Fig. 7), which yielded the result of 5.4 ± 0.12 meV.

Figure 8 shows the measured electron mobility as a function of temperature for the Sb-doped (2%) ZnO sample grown with P (O_2) = 1.3 Pa. Look *et al.*[24] have developed a formalism to determine the donor and acceptor concentrations (N_D and N_A, respectively) from the mobility data in a degenerate

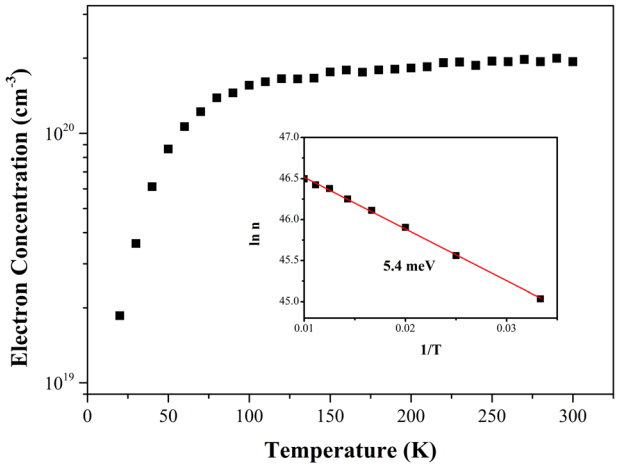

FIG. 7. The electron concentration against the temperature for the as-grown Sb-doped sample (Sb = 2%) grown with the oxygen pressure of 1.3 Pa. The inset shows the corresponding Arrhenius plot at temperatures from 10 K to 150 K, and the fitted straight yielding the ionization energy of the shallow donor.

semiconductor thin film system. The mobility is limited by ionized impurity scattering (ii), phonon scattering (ph), and charged grain boundary (bdry), and the total mobility is given by Matthiessen's rule $\mu_{tot}{}^{-1} = \mu_{ii}{}^{-1} + \mu_{ph}{}^{-1} + \mu_{bdry}{}^{-1}$. The mobility limited by ionized impurity scattering is given by[25]

$$\mu_{ii}(n, N_{ii}) = \mu_{ii0}(n) n / Z^2 N_{ii}, \tag{1}$$

$$\mu_{ii0}(n) = \frac{24\pi^3 \varepsilon_0^2 \hbar^3}{e^3 m^{*2}} \frac{1}{\ln[1 + y(n)] - \frac{y(n)}{1 + y(n)}}, \tag{2}$$

where $y(n) = \frac{3^{1/3} 4\pi^{8/3} \varepsilon_0 \hbar^2 n^{1/3}}{e^2 m^*}$. ε_0 is the static dielectric constant, ħ is the Planck's constant divided by 2π. m^*, e is the effective mass and charge of the electron, respectively, N_{ii} is the concentration of the ionized impurity having the charge of Z, and n is the electron concentration of the sample.

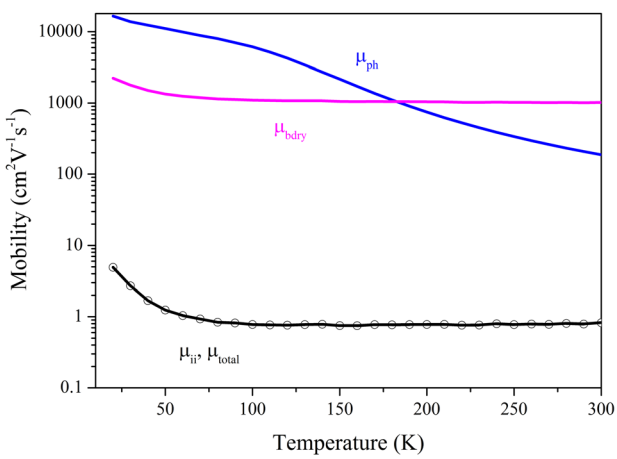

FIG. 8. Experimental mobility of the as-grown ZnO:Sb (2%) sample (dots) as a function of the temperature. The simulated curves are the mobilities limited by phonon scattering μ_{ph}, boundary scattering μ_{bdry}, ionized impurity μ_{ii}, and the total mobility calculated by the Matthiessen's rule μ_{total}. Notice that the curves of μ_{ii} and μ_{total} are effectively the same.

The optical phonon scattering limited mobility is given by[26]

$$\mu_{po}(T) = \frac{2^{\frac{3}{2}}\pi\hbar^2\left(\exp\left[\frac{T_{po}}{T}\right]-1\right)\chi(T_{po}/T)}{e(kT_{po})^{\frac{1}{2}}(m^*)^{\frac{3}{2}}(\varepsilon_1^{-1}-\varepsilon_0^{-1})}, \quad (3)$$

where T_{po} is the polar-optical temperature, k is the Boltzmann's constant, T is the measured temperature, and ε_1 is the high frequency dielectric constant. For ZnO at T ≈ 0–300 K, $\chi(T_{po}/T) = [1+\exp(-0.6T_{po}/T)]^{-1}$. The expression of acoustic phonon scattering limited mobility is given by[22]

$$\mu_{ac}(n,T) = \frac{\pi\hbar^4 c_l}{2^{\frac{1}{2}}(m^*)^{\frac{5}{2}}E_l^2 ekT}E_f(n)^{-1/2}, \quad (4)$$

where c_l and E_l are the longitudinal elastic constant and acoustic deformation potential, respectively. $E_f(n)$ is the Fermi-energy, which is given by $E_f(n) = \hbar^2(3\pi^2 n)^{2/3}/2m^*$. The mobility limited by acoustic phonon interacting through the piezoelectric potential is[27]

$$\mu_{pe}(n,T) = \frac{2^{3/2}\pi\hbar^2\mathcal{E}_0}{(m^*)^{3/2}P_{pe}^2 ekT}E_f(n)^{1/2}, \quad (5)$$

where P_{pe} is the piezoelectric constant. The phonon limited mobility is associated with these three phonon processes, i.e., $\mu_{ph}^{-1} = \mu_{po}^{-1} + \mu_{ac}^{-1} + \mu_{pe}^{-1}$.

The mobility limited by scatterings at the boundary, interface, and surface is given by[25,28]

$$\mu_{bdry}(d,n,C) = \frac{e}{\hbar}\frac{d/C}{(3\pi^2 n)^{1/3}}, \quad (6)$$

where d is the film thickness and C is a constant dependent on the film/substrate system.

By combining the above equations, the donor and acceptor concentration can be solved as[24]

$$N_D = \frac{n}{Z_D(Z_D+Z_A)}\times\left\{\frac{\mu_{ii0}(n)}{\mu_{expt}(T)}[1-Corr(d,n,C,T)]+Z_A\right\}, \quad (7)$$

$$N_A = \frac{n}{Z_A(Z_D+Z_A)}\times\left\{\frac{\mu_{ii0}(n)}{\mu_{expt}(T)}[1-Corr(d,n,C,T)]-Z_D\right\}, \quad (8)$$

where $Corr(d,n,C,T) = \frac{\mu_{expt}(T)}{\mu_{ph}(n,T)} + \frac{\mu_{expt}(T)}{\mu_{bdry}(d,n,C)}$, Z_A and Z_D is the charge state of the acceptor and donor, respectively, and $\mu_{expt}(T)$ is the experimental mobility.

To carry out the simulation, the following values were taken, namely, $T_{po} = 837$ K, $\varepsilon_1 = 3.72\,\varepsilon_{vac}$ and $\varepsilon_0 = 8.12\,\varepsilon_{vac}$, $c_1 = 1.4\times10^{11}$ Nm^{-2}, $E_1 = 3.8$ eV, and $m^* = 0.32m_0$ (see references in Ref. 19). The film thickness was taken to be $d = 300$ nm. C was taken to be 2.5, referring to the value obtained in ZnO grown by PLD on sapphire.[28] The generated modeled curves of μ_{ph}, μ_{bdry}, and μ_{ii} as well as the resultant mobility μ_{total} are shown in Fig. 8. The simulated resultant mobility curve well fitted the experimental data. It is also noticed from Fig. 8 that the dominant scattering process limiting the mobility was ionized impurity scattering throughout the whole measured temperature range from 10 K to 300 K ($\mu_{ii}^{-1} \cong \mu_{tot}^{-1} = \mu_{ii}^{-1} + \mu_{ph}^{-1} + \mu_{bdry}^{-1}$ as μ_{ii}^{-1} is much larger than μ_{ph}^{-1} and μ_{bdry}^{-1}).

The donor and acceptor concentrations of the sample can be calculated by Eqs. (7) and (8) with the input of their charges Z_A and Z_D. Concerning the compensating acceptor, Tuomisto *et al.*[29] showed by PAS that V_{Zn} was the dominant compensating acceptor in n-type ZnO. Moreover, Look *et al.*[24] reported the dramatic enhancement of V_{Zn} in degenerately n^+ Ga-doped ZnO having a $n \sim 10^{21}$ cm^{-3} Ga-doped ZnO sample fabricated by PLD by the effect self-compensation. For the present n^+ sample with the Fermi level very close to the conduction band minimum (CBM), V_{Zn} would possess a charge of 2-, as it has the acceptor states of (0/-) and (-/2-) states in the band gap. For the Sb-doped ZnO sample, Sb_{Zn}-$2V_{Zn}$[9] and Sb_i–$3V_{Zn}$[23] are also acceptors that can compensate the electron concentration. Sb_{Zn}-$2V_{Zn}$ thus would possess a charge state of 3- as Sb_{Zn}-$2V_{Zn}$ has two states of (0/-) and (-/3-) in the band gap, and Sb_i–$3V_{Zn}$ would possess a charge state of 1- as it has a (0/-1) state in the band gap. The shallow donor responsible for the n^+ conductivity as found in the as-grown Sb-doped ZnO in the present study had an ionization energy of ∼5 meV. Residual shallow donors in undoped ZnO usually had an ionization energy of ∼ 30 meV. It has been attributed to H[5] (charge state of +1), and an intrinsic defect complex like Zn_i-N_O[6] (having (0/+) level in the band gap and thus a charge state of +1), which had a charge state of +1. The shallow donor as found in the as-grown Sb-doped ZnO sample in the present study, which has an ionization energy of ∼5 meV, is unlikely the residual shallow donor commonly found in undoped ZnO materials. A theoretical study showed that Sb_{Zn} was a deep donor[14] having a state (3+/+) in the band gap but the level was deep, but there exists also literature attributing the n^+ conductivity of Sb-doped ZnO to the Sb_{Zn}.[30] Though the charge states of the donor Z_D and acceptor Z_A are not exactly known, it is still worthy to estimate the values of Z_A and Z_D from Eqs. (7) and (8) by taking the values of Z_D and Z_A equal to 1, 2, and 3, respectively, and the results are shown in Table I. Thus, from the table, N_D and N_A are in the ranges of 3.2×10^{19}–2.7×10^{20} cm^{-3} and 2.6×10^{19}–2.5×10^{20} cm^{-3}, respectively. A very high acceptor concentration N_A (∼2×10^{19}–2×10^{20} cm^{-3}) was obtained in this as-grown ZnO:Sb (2%) sample having n^+ ∼4×10^{20} cm^{-3}. A similarly high concentration of V_{Zn} has been reported by Look *et al.*[19] in Ga-doped ZnO (Ga concentration = 1.4×10^{21} cm^{-3}) grown by PLD on sapphire. This was attributed to the self-compensation,[24] which was associated with the significant decrease of the formation energy V_{Zn} as the Fermi level was degenerately close to the conduction band.

C. Positron annihilation spectroscopic studies

Because of its selective sensitivity towards Zn-vacancy related defects in ZnO,[29,31] the PAS study was performed on the Sb-doped ZnO samples (Sb = 2% and P (O_2)=1.3 Pa)

TABLE I. The concentrations of donor N_D and acceptor N_A for the as-grown ZnO:Sb (2%) sample estimated from the mobility data taking different possible charge states of the donor and acceptor (Z_D and Z_A).

	N_A (cm^{-3})	N_D (cm^{-3})
$Z_A = 1; Z_D = 1$	2.5×10^{20}	2.7×10^{20}
$Z_A = 1; Z_D = 2$	1.6×10^{20}	9.0×10^{19}
$Z_A = 1; Z_D = 3$	1.2×10^{20}	4.5×10^{19}
$Z_A = 2; Z_D = 1$	8.4×10^{19}	1.9×10^{20}
$Z_A = 2; Z_D = 2$	6.1×10^{19}	7.0×10^{19}
$Z_A = 2; Z_D = 3$	4.7×10^{19}	3.8×10^{19}
$Z_A = 3; Z_D = 1$	4.2×10^{19}	1.5×10^{20}
$Z_A = 3; Z_D = 2$	3.3×10^{19}	5.8×10^{19}
$Z_A = 3; Z_D = 3$	2.6×10^{19}	3.2×10^{19}

annealed at different annealing temperatures up to 900 °C so as to investigate the thermal evolution of Zn-vacancy related defects in the Sb-doped samples. The principal of PAS is that the outgoing positron-electron annihilation gamma photons carry the information of the electronic environment nearby the positron annihilation.[31,32] Depth profiling of Zn-vacancy related defects was obtained by scanning the positron incident energy and the mean positron implantation depth (in nm) was given by $\overline{x} = (40/\rho)E^{1.6}$,[31,32] where ρ is the material density in g/cm^3 and E is the positron incident energy in keV. The Doppler broadening of the annihilation peak in the gamma ray energy spectrum was parameterized by the S-parameter (as defined in the section Experimental). The measured S-parameter is the weighted contribution from the corresponding annihilation site, i.e., $S(E) = \sum_i f_i(E) S_i$, where f_i (E) and S_i are, respectively, the fraction of positrons annihilating at and the characteristic S-parameter of the i-th annihilation site The S-parameter as a function of the positron incident energy for the different samples (as-grown undoped and Sb-doped samples annealed at different temperatures) is shown in Fig. 9.

As shown in Fig. 9, the S (E) plots of all the samples showed similar features. The S-parameter first decreased with increasing E (i.e., implantation depth) as the characteristic surficial S-parameter was larger than that of the sample ZnO film. The S-parameter then reached a plateau at 2.5 keV $< E <$ 7 keV, which referred to the majority of incident positrons annihilated in the sample film. Further increasing E would inject positrons into the sapphire substrate and would lead to the decrease of the S-parameter as the characteristic S-parameter of sapphire is lower than that of ZnO. The S-parameter finally saturated at a large E as a majority of the incident positrons annihilated in the sapphire substrate. The S-parameters of the different ZnO film samples were thus taken at the positron incident energy of 5 keV. This corresponded to a mean depth of ~100 nm which was at the mid of the ZnO film.

The S-parameter of the Sb-doped ZnO (Sb = 2% and grown at 1.3 Pa) samples against the annealing temperature was plotted in Fig. 10, and the electron concentration was also included here for comparison. The dramatic decrease of electron concentration after annealing at 750 °C (4×10^{20} cm^{-3} for the as-grown sample to 5×10^{16} cm^{-3} after annealing) is well correlated with the increase of the S-parameter.

Coincidence Doppler broadening (CDB) measurement is a PAS technique capable of offering electronic momentum distribution and thus the information of the chemical environment around the site that the positrons annihilate.[31,32] In order to study the microstructure of the Zn-vacancy related defects in the Sb-doped ZnO samples, CDB measurements were conducted. The electronic momentum distribution ratio curves of the Sb metal, the undoped ZnO film sample, the as-grown ZnO:Sb (Sb = 1%–3%), and the ZnO:Sb (2%) film samples annealed at different temperatures were normalized against the Bridgman grown ZnO single crystal, and the results are shown in Fig. 11. The ZnO single crystal is very close to the positron trap as compared to the PLD grown ZnO samples. The regions of the windows used for calculating the S and the W-parameters are also included in the figure for reference. A peak centered at around $p_z = 0$ was found in the ratio curve for the Sb sample, and was thus the fingerprint feature of the positron annihilating with the valence electrons of the Sb atom. Another feature of the Sb-metal is that it has a very low distribution of electrons having a high momentum ($p_L > 10 \times 10^{-3}$ m_0c) as compared to the ZnO bulk (the reference sample taken as unity).

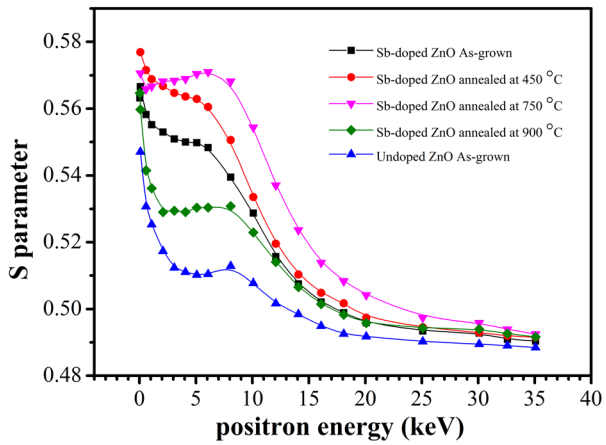

FIG. 9. The S parameter as a function of incident positron energy for the as-grown undoped ZnO sample and the ZnO:Sb (2%) samples annealed at different temperatures. All the samples were grown at the oxygen pressure of 1.3 Pa.

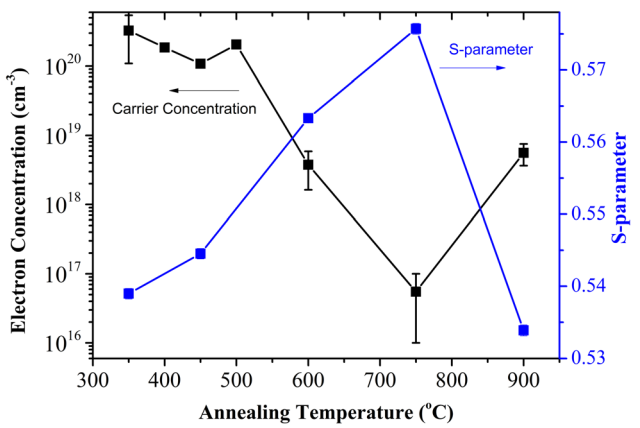

FIG. 10. Electron concentration and S-parameter as a function of the annealed temperature for the ZnO:Sb (2%) samples grown at the oxygen pressure of 1.3 Pa.

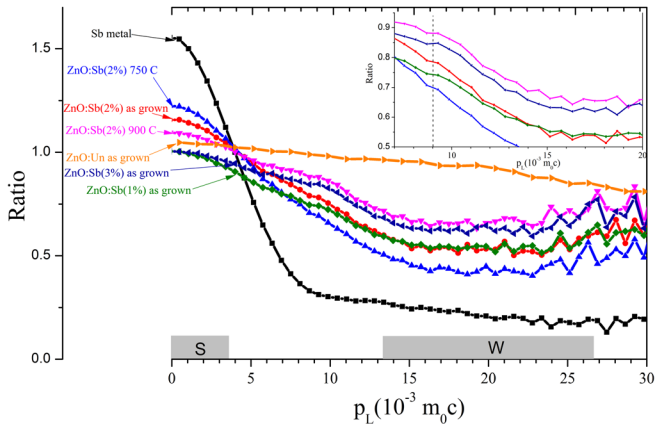

FIG. 11. The ratio curves of the electronic momentum distribution obtained from the CDB measurement for the undoped ZnO sample and the ZnO:Sb samples with different Sb compositions and annealed at different temperatures. All the samples were grown with the oxygen pressure of 1.3 Pa. The legends shown are ranked according to the intensity of the Sb-related peak at $p = 0$.

Similar features (i.e., peak at $p_L = 0$ and low count at high p_L) were also observed in the ratio curves of all the annealed Sb-doped ZnO samples but not observed in those of the undoped ZnO sample. The Sb-related peak of the ratio curves for the Sb-doped ZnO samples was associated with positrons annihilating in the Zn-vacancy complex decorated with the Sb, while the peak intensities reflected the concentration of this defect complex. The increase of the S-parameter after annealing at 750 °C (Fig. 10) can thus be understood as the increase of the count in the S-parameter window of the CDB spectra, which is characteristic of the positron annihilating with the Sb atom.

As shown in the ratio curves in Fig. 11, the intensity of the Sb related peak for the ZnO:Sb (2%) sample was enhanced after annealing at 750 °C, and then decreased after annealing at the higher temperature of 900 °C. It is noticed that the electron concentration anti-correlates with the Sb-related peak intensity in the CDB spectra. It is thus suggested that these electron concentration drops induced by 750 °C annealing are related to the V_{Zn}-Sb defect complex detected by CDB spectroscopy, which acts as the compensating defect. It was also worthy to point out that some V_{Zn}-Sb defect complex already existed in the as-grown sample. With first principles calculation, Limpijumnong *et al.*[14] suggested that Sb_{Zn}-$2V_{Zn}$ was a shallow acceptor having a low formation energy. Puchaia and Morgan[23] reported that Sb_i–$3V_{Zn}$ was the stable deep acceptor in ZnO. These two acceptor defect complexes could be the candidate of the V_{Zn}-Sb complex, though only the present CDB data cannot offer information for distinguishing its exact microstructure between these two defect complexes.

D. XPS study

XPS study was performed to study the chemical states of Sb in the ZnO:Sb samples. Figures 12(a)–12(c), respectively, show the XPS spectra of the Sb $3d_{3/2}$ state of the as-grown ZnO:Sb (2%) sample and those upon annealing at 750 and 900 °C. The $3d_{3/2}$ peaks were fitted by the Sb^{3+} and Sb^{5+} peaks locating at ~540.2 eV and 540.8 eV, respectively.[33] The fitted intensity ratios of the peaks Sb^{5+}/Sb^{3+} are 1.61, 4.82, and 2.33 for the as-grown, 750, and 900 °C annealed ZnO:Sb samples, respectively. The maximum Sb^{5+}/Sb^{3+} intensity ratio at the annealing temperature of 750 °C well anti-correlates with the minimum of the electron concentration (see Fig. 6), for which the discussion will be given in the upcoming Discussion section. The Zn $2p_{3/2}$ XPS spectrum located at 1021.9 eV of the ZnO:Sb (2%) with different annealing conditions is shown in Fig. 12(d), for which no significant difference is found among these spectra.

E. PL study

Figure 13 shows the near band edge emission (NBE) of the low temperature (10 K) PL spectra for the as-grown ZnO:Sb (2%) samples and that annealed at 750 °C. The peak at 3.36 eV is found in both samples, and a similar peak has

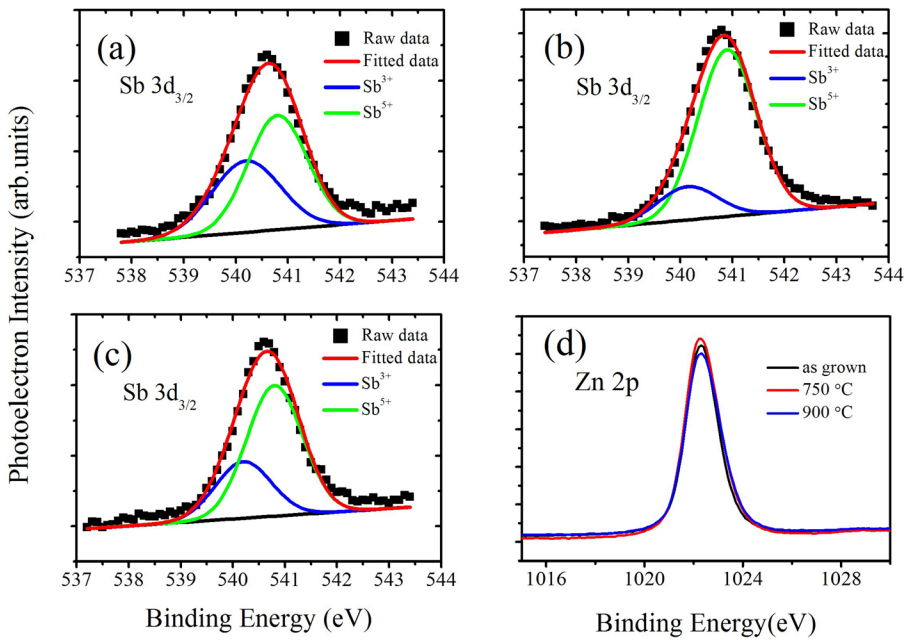

FIG. 12. The XPS spectra of the ZnO:Sb (2%) films: the Sb $3d_{3/2}$ state for (a) the as-grown, (b) those annealed at 750 °C, and (c) annealed at 900 °C; (d) the Zn $2p_{3/2}$ state. The samples were grown with P $(O_2) = 1.3$ Pa. The Sb $3d_{3/2}$ peaks were fitted by two Gaussian peaks, namely, associated with the Sb^{3+} and Sb^{5+} states.

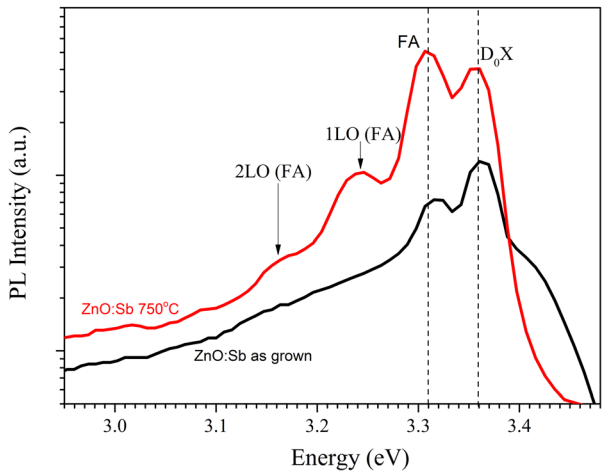

FIG. 13. The PL spectra for the as-grown ZnO:Sb (2%) and those annealed at 750 °C. These sample were grown under P $(O_2) = 1.3$ Pa.

been assigned to the neutral donor bound exciton (D^0X) emission (Refs. 1 and 35 and references therein). The shoulder at ~3.42 eV was only observed in the as-grown ZnO:Sb sample, which has been reported to be associated with the A free exciton first excited-state transition $FX_A^{n=2}$.[36] For the as-grown ZnO:Sb sample, a PL emission at 3.32 eV is found and its intensity is lower than the D^0X emission. After annealing at 750 °C, this emission slightly red-shifts to 3.31 eV and its intensity is higher than that of the D^0X line. Emission at around 3.32 eV has been associated to the two-electron satellite (TES) transition of the neutral donor bound exciton (Refs. 1 and 35 and references therein). However, the 3.31 eV emission as seen in the annealed ZnO:Sb sample is not likely due to the TES as the TES emission has an intensity lower than the D_0X emission. The 3.32 eV emission as seen in the annealed ZnO:Sb sample is suggested to have originated from the free-to-acceptor (FA) transition. Emissions of 3.25 eV and 3.17 eV are also observed in the annealed ZnO:Sb sample, and these lines are attributed to the first and second phonon replica (1LO and 2LO, respectively) of the FA emission as they are separated by ~70 meV. The acceptor binding energy was calculated by $E_A = E_g - E_{FA} + kT/2$, where $E_g = 3.44$ eV and $E_{FA} = 3.32$ eV, and a value of $E_A = 0.12$ eV was yielded. For the as-grown ZnO:Sb sample, it is difficult to distinguish whether the 3.31 eV emission (which is slightly bluer than the FA found in the as-grown ZnO:Sb sample) is associated with the TES or the FA. Nevertheless, it is plausible to conclude that annealing the ZnO:Sb sample at 750 °C enhances the FA emission associated with the shallow acceptor with a binding energy of 120 meV.

IV. DISCUSSION

The undoped ZnO sample has $n \sim 1 \times 10^{18}$ cm^{-3}, and all the as-grown Sb-doped ZnO samples with Sb = 0.5% to 2% are n^+ conductive having an electron concentration larger than $\sim 10^{20}$ cm^{-3}. For the high Sb composition of 3%, the carrier drops abruptly and the sample becomes highly resistive. For the low Sb composition ≤ 2%, the electron concentration of the as-grown ZnO:Sb samples increases with the Sb doping composition and is effectively equal to the Sb concentration. In addition, the ionization energy of the shallow donor is ~5 meV, which is not close to that found in the undoped ZnO materials.[5,6] It is thus plausible to associate the n^+ conductivity to the Sb related shallow donor. Substitutional defects of Sb into Zn-site Sb_{Zn} and O-site Sb_O are, respectively, the donor and acceptor. The first principle calculations showed that the Sb_{Zn} was a deep donor.[14] However, similar to the findings in the present study, Liu *et al.*[30] and Heo *et al.*[34] observed n^+ type conductivity in Sb-doped and P-doped ZnO with a relatively low doping composition, and the materials became highly resistive as the dopant compositions were high. The shallow donors responsible for the n^+ conductivity were attributed to the Sb and P substitutional defect of the Zn-site or the relevant defect complex. In the present study, the temperature dependent measurement revealed that the shallow donor had an ionization energy of ~5 meV, and was unlikely associated with the shallow donors like hydrogen or the intrinsic defect complex which had an ionization energy of ~35 meV.[6,35] The ionic radius of Sb^{3-} of 2.44 Å is much larger than that of O^{2-} (1.38 Å) (see references in Ref. 34). The ionic radii of Zn^{2+} and Sb^{3+} are close to each other and having values of 0.74 Å and 0.62 Å, respectively (see references in Ref. 34). The Sb dopant is thus more likely to occupy the Zn-site of the ZnO lattice, whereas Sb_{Zn} is a donor type defect. Using the conversion-electron emission channeling from radioactive Sb and As, Wahl *et al.*[15] studied the Sb and As-implanted ZnO single crystal with the Sb concentration $\approx 2 \times 10^{19}$ cm^{-3} (estimated from the dose and implantation given), which was lower than that of all the present Sb-doped ZnO samples. It was found that the majority of the Sb and As occupied the Zn site of the ZnO lattice. It is plausible to attribute the shallow donor responsible for the n^+ conductivity in the ZnO:Sb samples with Sb ≤ 2% of the present study to the Sb_{Zn} or its complex defect.

An annealing study of the ZnO:Sb sample with Sb = 2% shows that annealing at 750 °C, significantly reduces the material electron concentration by larger than the factor of 1000. The electron concentrations for the undoped ZnO grown by the same PLD system, similar growth parameters, and annealing temperatures are in the range of 10^{18}–10^{19} cm^{-3}. As the electron concentration of the ZnO:Sb (2%) grown with $P(O_2) = 5$ Pa dropped from 10^{20} cm^{-3} to 10^{14} cm^{-3} after annealing at 750 °C, the electron concentration drop cannot be solely due to the removal of the Sb_{Zn} but must be originated to the formation of compensating defects with concentration $\sim 10^{20}$ cm^{-3}. The concentration of V_{Zn} (10^{19}–10^{20} cm^{-3}) was enhanced in the as-grown degenerate ZnO:Sb (say 2%) with $n^+ \sim 10^{20}$ cm^{-3} due to the self-compensation effect while the Fermi level was close to the conduction band and thus the formation energy of V_{Zn} was low. However, the V_{Zn} concentration in the ZnO:Sb sample annealed at 750 °C cannot be as high as $\sim 10^{20}$ cm^3 because the E_F is not close to the E_C and the formation energy of V_{Zn} is not lowered by the self-compensation effect. Thus, the compensating defect formed upon annealing at 750 °C cannot be V_{Zn}.

The annealing inducing a drop of electron concentration well correlates with the increase of the V_{Zn}-Sb defect

concentration as detected by the CDBS. Theoretical studies using local density approximation (LDA) and generalized gradient approximation (GGA)[14,23] reported that the Sb_{Zn} substitutional defect was a deep donor, and the Sb_{Zn}-$2V_{Zn}$ defect complex was a shallow acceptor having a low formation energy and an ionization energy of $\varepsilon(0/-) = 0.16$ eV. With *ab initio* calculations, Puchala and Morgan[23] showed that the Sb_i–$3V_{Zn}$ defect complex was energetically stable and was a deep acceptor at $\varepsilon(0/-) = 0.28$ eV. The drop of the electron concentration induced by the 750 °C annealing is thus attributed to the formation of annealing induced formation of the V_{Zn}-Sb defect complex like the Sb_{Zn}-$2V_{Zn}$ or the Sb_i–$3V_{Zn}$ acceptors which compensate the free carrier. Further increasing the annealing temperature led to an increase of the electron concentration of the ZnO:Sb sample. This could be due to thermal dissociation of the V_{Zn}-Sb acceptor complex, which is evidenced by the drop of the Sb-related peak intensity in the CDB spectra after the annealing at 900 °C.

In previous systematic studies of ZnO:As grown on the Si substrate using the radio frequency sputtering technique,[18,19] the XPS study showed that a majority of the As dopant occupied the Zn site of the ZnO lattice. The as-grown ZnO:As sample was n-type and annealing at 600 °C converted the conductivity to p-type with a hole concentration of 6×10^{17} cm^{-3}. The annealing induced p-type conductivity was associated with the formation of the As_{Zn}-$2V_{Zn}$ shallow acceptor complex. Increasing the annealing temperature to 800 °C changed the conductivity to n-type and this was associated with the dissociation of the As_{Zn}-$2V_{Zn}$ shallow acceptor complex. The annealing temperature for the dissociation of the As_{Zn}-$2V_{Zn}$ defect was estimated by its theoretical binding energy[19] and the value was found to be 800 °C, which was close to the present observed temperature of 900 °C.

It is noticed from Fig. 3(a) that the lattice constant of the ZnO (002) peak dropped slightly after annealing at 750 °C, which is the annealing temperature for enhancing the V_{Zn}-Sb acceptor complex formation (Sb_{Zn}-$2V_{Zn}$ or Sb_i–$3V_{Zn}$) and suppressing the electron concentration. If the V_{Zn}-Sb acceptor complex formed is the Sb_i–$3V_{Zn}$ defect, it is expected that the formation of the Sb interstitial would introduce an increase of the lattice constant of the ZnO (002) peak, but the opposite trend is observed. It is more likely that the involved thermally created acceptor complex is the Sb_{Zn}-$2V_{Zn}$ shallow acceptor.

The XPS study on the chemical state of Sb in the ZnO:Sb (2%) samples upon different annealing temperatures showed that the Sb^{5+}/Sb^{3+} ratio in the samples anti-correlates with the electron concentration and correlates with the V_{Zn}-Sb acceptor complex concentration. Pandey *et al.*[33] carried out the XPS study on Sb-doped ZnO fabricated by dual ion beam sputtering and a high Sb^{5+}/Sb^{3+} ratio was correlated with the hole concentration, and thus the Sb_{Zn}-$2V_{Zn}$ shallow acceptor. This result is consistent with the assignment of the V_{Zn}-Sb acceptor complex to Sb_{Zn}-$2V_{Zn}$, rather than Sb_i–$3V_{Zn}$ as Sb_i–$3V_{Zn}$ is a deep acceptor.

Annealing the ZnO:Sb (2%) sample at 750 °C enhances the FA peak (at 3.31 eV) in the PL spectrum, and the corresponding acceptor has the binding energy of ~120 meV, which compensated the n^+ conductivity and revealed the CDB spectra. As the acceptor is shallow rather than deep, it should be Sb_{Zn}-$2V_{Zn}$ rather than Sb_i–$3V_{Zn}$. The binding energy of this acceptor is 120 meV, though not exactly matching but close to the value of $\varepsilon(0/-) = 160$ meV of Sb_{Zn}-$2V_{Zn}$ as obtained from first principles calculation.[14]

Despite the Sb_{Zn}-$2V_{Zn}$ acceptor being formed after annealing at 750 °C, the resulting samples were n-type rather than p-type. This could be due to the compensation of holes by the donors and/or deep traps (intrinsic or impurity defect) remaining in the annealed samples. SIMS measurement was conducted on the ZnO:Sb (2%) grown at P (O_2) = 1.3 Pa with annealing at 750 °C, and the H concentration remained at quite a high level of 3×10^{19} cm^{-3}.

While fixing the Sb composition at 1%, the electron concentration grown with $P(O_2) = 0$ is 5×10^{20} cm^{-3} and it drops with increasing oxygen pressure during growth (see Fig. 5). The electron concentration then saturated at P (O_2) = 1.3 Pa with n ~$9\times$ 10^{19} cm^{-3}. This could be due to the increase of the concentrations of V_{Zn} and/or its related acceptor like Sb_{Zn}-$2V_{Zn}$ as a result from increasing the oxygen growth pressure, which then compensated the free electrons.

The electron concentration increases with the Sb concentration for Sb composition $\leq$2%, but it dropped abruptly as the Sb composition increases to 3% (which referred to the Sb concentration of 8×10^{20} cm^{-3}, as seen in Fig. 4). The increase of electron concentration with the Sb concentration can be easily understood as the increase of the Sb_{Zn} related shallow donor, but this cannot explain the abrupt change of the sample to highly resistive as the Sb composition further increases to 3%. This could be due to the formation of a compensation defect which was associated with the distortion of the lattice structure like Sb_O (which had a large mismatch in the lattice constant) or interstitial.

Liu *et al.*[30] studied the Sb dopant defect in Sb-doped ZnO grown by plasma enhanced MBE. The conductivity changed from ~10^{20} cm^{-3} to ~10^{17} cm^{-3} as the Sb cell temperature was raised to ~475 °C (which approximately corresponded to the Sb composition of 1 at. %, i.e., 4.4×10^{20} cm^{-3}). The lattice constant and the FWHM of the ZnO (002) peak of the XRD spectra remained constant as the Sb cell temperature was in the range of 370 °C to 475 °C. It was because the ionic radius of Sb^{3+} was close to that of Zn^{2+} and thus the incorporation of Sb into the Zn site to form the shallow donor would not deteriorate the lattice structure. However, the lattice constant and the FWHM of the (002) peak increase significantly as the Sb cell temperature increased to 475 °C. It was explained by the occupation of the Sb atom into the O site rather than the Zn site for a high Sb concentration $\geq 4.4 \times 10^{20}$ cm^{-3}, as there was a large mismatch between the ionic radii of Sb^{3-} (2.44 Å) and O^{2-} (1.38 Å). The Sb_O (which was the deep acceptor) or its related complex thus compensates the electron concentration for the Sb-doped ZnO samples with a high Sb concentration. Similar correlated carrier compensation, and increases in the lattice constant and FWHM of the ZnO (002) peak are observed in the present study with a limiting Sb concentration of 8×10^{20} cm^{-3}, which is also close to that found by

Liu *et al.*[30] It is thus plausible to associate the carrier compensation observed at the limiting Sb composition of 3% (i.e., Sb concentration$\sim 8\times10^{20}\,cm^{-3}$) to the formation of the Sb_O acceptor or its related defect complex. However, the physics behind the change of the Sb occupation from the Zn site to the O site as the Sb concentration is high is not yet understood and requires further investigation.

The variation of the Sb_{Zn}-$2V_{Zn}$ peak intensity in the CDB spectra (Fig. 11) with the change of the Sb composition in the as-grown ZnO:Sb samples can also be understood with the formation of Sb_O with a large Sb composition. As shown in Fig. 11, the Sb_{Zn}-$2V_{Zn}$ related peak intensity increases as the Sb composition increases from 1% to 2%. It is because for the case of Sb $\leq$ 3%, Sb occupies the Zn site and thus increasing the Sb composition increases the chance of forming the Sb_{Zn}-$2V_{Zn}$ defect complex. As the Sb composition further increases to 3%, the Sb_{Zn}-$2V_{Zn}$ related peak intensity decreases because Sb starts occupying the O site for a high Sb composition and thus suppressing the formation of the Sb_{Zn}-$2V_{Zn}$ defect complex.

Another interesting feature is also noticed in the CDB spectra of the Sb-doped ZnO samples. A shoulder is observed at $p_L\sim9\times10^{-3}\,m_0c$ ($\sim$1.2 a.u.) in the CDB spectra all of the Sb-doped ZnO samples, but except the ZnO:Sb (2%) sample annealed at 750 °C in which the shoulder is barely observable. The corresponding magnified spectra are shown in the inset of Fig. 11. Makkonen *et al.*[37] calculated the ratio curves of different V_{Zn}-related defects in ZnO. A similar shoulder was found in the calculated ratio curves of V_{Zn} and $V_{Zn}V_O$, for which the two calculated ratio curves were very close and thus experimental distinguishing is not feasible. This shoulder was originated from the positron trapped at V_{Zn} and annihilating with the Zn cation electron. The absence of the shoulder in the ZnO:Sb (2%) sample annealed at 750 °C can be explained by the fact that there is negligibly isolated V_{Zn} and a majority of V_{Zn} is bound with Sb_{Zn} to form the Sb_{Zn}-$2V_{Zn}$, and thus positrons trapped in the V_{Zn} open volume annihilate with the Sb atom rather than the Zn atom. The ZnO:Sb (2%) sample annealed at 900 °C has a strong V_{Zn} related shoulder in the ratio curve (see the inset of Fig. 11). This observation supports the argument made in the previous paragraph that the Sb_{Zn}-$2V_{Zn}$ dissociates into Sb_{Zn} and V_{Zn} after annealing at 900 °C. The as-grown ZnO:Sb (3%) sample also has the strong V_{Zn} related shoulder. For the as-grown Sb doped ZnO samples with relatively low Sb compositions of 1% and 2%, the Sb_{Zn}-$2V_{Zn}$ defect complex already exists in the as-grown samples with some co-existence of isolated V_{Zn}. For the high Sb composition sample with Sb = 3%, the Sb starts occupying the O site as Sb_O. Thus, the formation of Sb_{Zn}-$2V_{Zn}$ is suppressed and there is more isolated V_{Zn}.

According to the S-parameter window as indicated and the peak intensity of ratio curves at $p_L = 0$ in Fig. 11, it can be observed that the ratio at the peak is well correlated with the measured S-parameter. The ratio of pure Sb at $p_L = 0$ is 1.55 as shown in Fig. 11, and that for the ZnO single crystal is unity. According to the ratio curves calculated by Makkonen *et al.*,[37] the ratio at $p_L = 0$ of V_{Zn} is about 1.08. As shown in Fig. 11, the ratios at $p_L = 0$ are 1.16, 1.22, and 1.09 for the ZnO:Sb (2%) as-grown, annealed at 750 and 900 °C. The S-parameters of the corresponding samples also follow the same trend *versus* the annealing temperature (as shown in Fig. 10). For the as-grown ZnO:Sb sample, the ratio at $p_L = 0$ is 1.16 which is larger than that of the V_{Zn}/$V_{Zn}V_O$ but smaller than the pure Sb, indicating that both V_{Zn} and Sb_{Zn}-$2V_{Zn}$ coexist in the as-grown sample. As the annealing temperature increases to 750 °C, the ratio at $p_L = 0$ increases to the maximum of 1.22 (and so does the S-parameter, as shown in Fig. 10), indicating the formation of the Sb_{Zn}-$2V_{Zn}$ shallow acceptor. Further increasing the annealing temperature 900 °C decreases the ratio at $p_L = 0$. This is due to the dissociation of the Sb_{Zn}-$2V_{Zn}$ into Sb_{Zn} and V_{Zn}. As the ratio at $p_L = 0$ of the ZnO:Sb sample upon annealing at 900 °C is 1.09, it is even lower than that of the as-grown ZnO:Sb sample (similar trend for the S-parameter in Fig. 10). This implies that a majority of the Sb_{Zn}-$2V_{Zn}$ has already been thermally dissociated to V_{Zn} after annealing at 900 °C.

V. CONCLUSION

Sb-doped ZnO films were grown on sapphire using the PLD method. The as-grown samples were n^+ conducting for the Sb concentration not exceeding the threshold concentration ($\sim 8\times10^{20}\,cm^{-3}$ for the present PLD grown samples at an oxygen pressure of 1.3 Pa) and the relevant shallow donor was proposed to be the Sb_{Zn} related defect. For high level Sb doping exceeding the threshold, Sb no longer occupied the Zn site but sat at the O site, and the resultant Sb_O was the deep acceptor which would compensate for the free carrier. Annealing the ZnO:Sb doped with a low Sb level lead to the formation of Sb_{Zn}-$2V_{Zn}$, which has been reported to be the shallow acceptor. The present result may explain why diverged results were obtained in studies of p-type doping of ZnO with Sb, as the yielded Sb-related defects depended on the Sb concentration. It also implied that too high of a doping level of Sb was not good for effective p-type doping, because the Sb dopant occupied the O-site if the doping level exceeded the threshold of Sb_O formation.

ACKNOWLEDGMENTS

This work was financially supported by the RGC GRF, HKSAR (Project No. 17302115), and the Guangzhou Science and Technology Project (2016201604030047).

[1]U. Ozgur, Y. I. Alivov, C. Liu, A. Teke, M. A. Reshchikov, S. Dogan, V. Avrutin, S. J. Cho, and H. Morkoc, J. Appl. Phys. **98**, 041301 (2005).
[2]C. H. Park, S. B. Zhang, and S. H. Wei, Phys. Rev. B. **66**, 073202 (2002).
[3]M. D. McCluskey and S. J. Jokela, J. Appl. Phys. **106**, 071101 (2009).
[4]Y. J. Zeng, Z. Z. Ye, W. Z. Xu, D. Y. Li, J. G. Lu, L. P. Zhu, and B. H. Zhao, Appl. Phys. Lett. **88**, 062107 (2006).
[5]C. G. Van de Walle, Phys. Rev. Lett. **85**, 1012 (2000).
[6]D. C. Look, G. C. Farlow, P. Reunchan, S. Limpijumnong, S. B. Zhang, and K. Nordlund, Phys. Rev. Lett. **95**, 225502 (2005).
[7]L. Liu, Z. Mei, A. Tang, A. Azarov, A. Kuznetsov, Q. K. Xue, and X. Du, Phys. Rev. B **93**, 235305 (2016).
[8]M. G. Wardle, J. P. Goss, and P. R. Briddon, Phys. B **376**, 731 (2006).
[9]X. B. Li, S. Limpijumnong, W. Q. Tian, H. B. Sun, and S. B. Zhang, Phys. Rev. B **78**, 113203 (2008).
[10]D. C. Look, G. M. Renlund, R. H. Burgener, and J. R. Sizelove, Appl. Phys. Lett. **85**, 5269 (2004).

[11]S. K. Pandey, S. K. Pandey, V. Awasthi, A. Kumar, U. P. Deshpande, M. Gupta, and S. Mukherjee, J. Appl. Phys. **114**, 163107 (2013).
[12]K. K. Kim, H. S. Kim, D. K. Hwang, J. H. Lim, and S. J. Park, Appl. Phys. Lett. **83**, 63 (2003).
[13]S. K. Pandey, V. Awasthi, S. Verma, M. Gupta, and S. Mukherjee, Curr. Appl. Phys. **15**, 479 (2015).
[14]S. Limijumnong, S. B. Zhang, S. H. Wei, and C. H. Park, Phys. Rev. Lett. **92**, 155504 (2004).
[15]U. Wahl, E. Rita, J. G. Correia, A. C. Marques, E. Alves, and J. C. Soares, Phys. Rev. Lett. **95**, 215503 (2005).
[16]U. Wahl, J. G. Correia, T. Mendonça, and S. Decoster, Appl. Phys. Lett. **94**, 261901 (2009).
[17]F. X. Xiu, Z. Yang, L. J. Mandalapu, D. T. Zhao, J. L. Liu, and W. P. Beyermann, Appl. Phys. Lett. **87**, 152101 (2005).
[18]J. C. Fan, C. Y. Zhu, S. Fung, Y. C. Zhong, K. S. Wong, Z. Xie, G. Brauer, W. Anwand, W. Skorupa, C. K. To, B. Yang, C. D. Beling, and S. Fung, J. Appl. Phys. **106**, 073709 (2009).
[19]C. K. To, B. Yang, S. C. Su, C. C. Ling, C. D. Belilng, and S. Fung, J. Appl. Phys. **110**, 113521 (2011).
[20]X. W. Sun, B. Ling, J. L. Zhao, S. T. Tan, Y. Yang, Y. Q. Shen, Z. L. Dong, and X. C. Li, Appl. Phys. Lett. **95**, 133124 (2009).
[21]Y. R. Ryu, T. S. Lee, and H. W. White, Appl. Phys. Lett. **83**, 87 (2003).
[22]A. Janotti and C. G. Van de Walle, Rep. Prog. Phys. **72**, 126501 (2009).
[23]B. Puchala and D. Morgan, Phys. Rev. B **85**, 195207 (2012).
[24]D. C. Look, K. D. Leedy, L. Vines, B. G. Svensson, A. Zubiaga, F. Tuomisto, D. R. Doutt, and L. J. Brillson, Phys. Rev. B **84**, 115202 (2011).
[25]D. C. Look, K. D. Leedy, D. H. Tomich, and B. Bayraktaroglu, Appl. Phys. Lett. **96**, 062102 (2010).
[26]D. Howarth and E. H. Sondheimer, Proc. R. Soc. A **219**, 53 (1953).
[27]D. Rode, Semicond. Semimetals **10**, 1 (1975).
[28]R. C. Scott, K. D. Leedy, B. Bayraktarouglu, D. C. Look, and Y. H. Zhang, Appl. Phys. Lett. **97**, 072113 (2010).
[29]F. Tuomisto, V. Ranki, K. Saarinen, and D. C. Look, Phys. Rev. Lett. **91**, 205502 (2003).
[30]H. Y. Liu, N. Izumskaya, V. Avrutin, Ü. Özgür, A. B. Yankovich, A. V. Kvit, P. M. Voyles, and H. Morkoç, J. Appl. Phys. **112**, 033706 (2012).
[31]F. Tuomisto and I. Makkonen, Rev. Mod. Phys. **85**, 1583 (2013).
[32]R. Krause-Rehburg and H. S. Leipner, *Positron Annihilation in Semiconductors-Defects Defects* (Springer, Berlin, 1999).
[33]S. K. Pandey, S. K. Pandey, V. Awasthi, M. Gupta, U. P. Deshpande, and S. Mukherjee, Appl Phys. Lett. **103**, 072109 (2013).
[34]Y. W. Heo, S. J. Park, K. Ip, S. J. Pearton, and D. P. Norton, Appl. Phys. Lett. **83**, 1128 (2003).
[35]Z. L. Wang, S. C. Su, M. Younas, F. C. C. Ling, W. Anwand, and A. Wagner, RSC Adv. **5**, 12530 (2015).
[36]A. Teke, Ü. Özgür, S. Dogan, X. Gu, H. Morkoc, B. Nemeth, J. Nause, and H. O. Everitt, Phys. Rev. B **70**, 195207 (2004).
[37]I. Makkonen, E. Korhonen, V. Prozheeva, and F. Tuomisto, J. Phys.: Condens. Matter **28**, 224002 (2016).